Abdominal Imaging

Published online: 29 January 2011

Abdom Imaging (2011) 36:300–314
DOI: 10.1007/s00261-011-9683-3

INVITED FEATURE SECTION

Assessment of the treatment response of HCC

Kyung Won Kim,[1] Jeong Min Lee,[1] Byung Ihn Choi[1,2]

[1]Department of Radiology, Seoul National University Hospital, 101 Daehangno, Jongno-gu, Seoul 110-744, Korea
[2]Institute of Radiation Medicine, Seoul National University Hospital, 101 Daehangno, Jongno-gu, Seoul 110-744, Korea

Abstract

Surgical hepatectomy or liver transplantation are considered as curative treatment modalities for hepatocellular carcinoma (HCC). However, many patients are not surgical candidates at the time of diagnosis. Great improvements in locoregional therapies including local ablative therapy [radiofrequency (RF) ablation or ethanol ablation] and transarterial techniques (transarterial embolization or transarterial radioembolization) have made possible local control of HCC. For unresectable HCC, a targeted therapy with sorafenib may improve survival. Unlike treatment of other oncologic tumor, the locoregional therapies are mainstay in the treatment of HCC. Therefore, the application of classical criteria such as the World Health Organization (WHO) guideline may not be suitable for accurate treatment response assessment of locoregional therapies or targeted therapy of HCC. An understanding of the imaging features of post-treatment imaging after various treatment modalities for HCC is crucial for treatment response assessment and for determining further therapy. In this article, we review the role of various imaging modalities in assessing treatment response of locoregional therapies and the targeted molecular therapy.

Key words: Hepatocellular carcinoma—Liver tumors—Radiofrequency ablation—Transarterial embolization—Sorafenib therapy

Hepatocellular carcinoma (HCC) is a major global health problem with an estimated incidence ranging between 500,000 and 1,000,000 new cases annually [1]. During the past two decades, liver transplantation and partial hepatectomy have been considered the main curative treatments. Liver transplantation is considered to be the only truly curative therapy for patients with HCC and liver cirrhosis (LC) because of the high risk of recurrent HCC in the native cirrhotic liver. However, the international shortage of liver donors, the strict patient selection criteria, and the high cost of surgical procedure limits the practical use of liver transplantation [2]. Currently, the reported overall 5-year patient survival after resection of HCC is 40%–70% with a continuing decrease in operative mortality [3]. Unfortunately, only 10%–30% of HCCs are amenable to "curative" surgical resection at the time of diagnosis because advanced disease with intrahepatic or extrahepatic tumor spread, gross vascular invasion or inadequate functional liver reserve related to co-existent cirrhosis precludes successful surgery [4]. In the past years, great improvements in locoregional therapies, including local ablative therapy [radiofrequency (RF) ablation, ethanol ablation or cryotherapy] and transarterial techniques (transarterial chemoembolization or transarterial radioembolization), have made possible local control of HCC. Currently, surgical treatment competes with various locoregional therapies as the first-line treatment option for patients with small HCCs with well-preserved liver function as well as for patients who are not candidates for surgical cure due to the severity of their liver disease or the advanced stage of their HCC [3]. In cases of advanced HCC without effective treatment options, systemic chemotherapy had not shown a beneficial effect on the survival rates until a multikinase inhibitor, sorafenib, increased overall patient survival when used as the targeted molecular therapy [5].

Assessment of tumor response after locoregional therapies and targeted molecular therapy is important in determining treatment success, identifying complications, and guiding future therapy. Various imaging modalities, such as computed tomography (CT), contrast-enhanced ultrasonography (CE-US), and magnetic resonance imaging (MRI), have a fundamental role in the treatment response monitoring of HCC. In this study, we review the role of various imaging modalities in assessing the treatment response of locoregional therapies and the targeted molecular therapies.

Correspondence to: Byung Ihn Choi; *email:* bichoi@snu.ac.kr

Role of imaging in assessing the treatment response of HCC

Traditionally, the primary measure of tumor response to therapy in most oncologic trials is change in tumor burden characterized by tumor size and number. In 1979, the World Health Organization (WHO) (bidimensional perpendicular measurements) published guidelines on the anatomic assessment of tumor response to therapy [6]. The Response Evaluation Criteria in Solid Tumors (RECIST) guidelines (unidimensional measurements) were published in 2000 [7] and were subsequently updated to the revised RECIST (version 1.1) guidelines [8]. While the original intent of the WHO and RECIST guidelines was to evaluate the change in tumor size following systemic chemotherapies and to disregard the extent of necrosis which is the target of all effective locoregional therapies, in systemic chemotherapy all tumors are theoretically equally exposed to systemic agents, although this approach does not translate directly to locoregional therapies which may not target all disease [9]. In RF ablation, the ablation zone should be larger than the index tumor with a sufficient safety margin, which may cause difficulty in assessing the treatment response according to the WHO or RECIST guidelines. Therefore, the European Association for the Study of the Liver (EASL) recommended the use of lesion enhancement on contrast-enhanced CT as the standard modality to determine the treatment response of HCC after locoregional therapy [10]. Areas of tumor enhancement were considered viable, whereas non-enhancing regions reflected tissue necrosis. According to the EASL guidelines, complete response (CR) was defined as the absence of enhanced tumor areas and thus reflecting complete tissue necrosis; partial response (PR) was defined as a decrease $>50\%$ of the enhanced areas and thus reflecting partial tissue necrosis; progressive disease (PD) was defined as an increase $>25\%$ in the size of a single, measurable lesion or the appearance of new lesions; and stable disease (SD) was defined as a tumor response between PR and PD [11].

Recent advances in the development of functional imaging techniques have provided the ability to detect microscopic changes in tumor microenvironment and microstructure, thus allowing the assessment of tumor response after locoregional treatment by observing alterations in tumor viability, perfusion or vascularity [12–14]. Diffusion-weighted MRI (DW-MRI) and the apparent diffusion coefficient (ADC) map reflect the water molecule diffusion in tissue and can discriminate viable tumor from necrotic tissue. Viable tumor cells have intact membranes that restrict water molecules, whereas necrotic tissue shows increased water molecule diffusion due to cell membrane disruption [15]. Perfusion CT or dynamic contrast enhancement MR can assesses the change in tumor vascularity and perfusion after TACE or local ablation therapy [13, 16, 17]. Recently, color mapping of the arterial enhancement fraction was developed in order to be used as a surrogate marker for perfusion CT [18]. However, these functional imaging techniques have not been standardized which impedes its use in the treatment response assessment of HCC [9].

New contrast agents are now being developed to increase the efficacy of the detection and characterization of liver tumors. The two new contrast agents, Gd-BOPTA (Gadobenate dimeglumine, Multihance®; Bracco Italy) and Gd-EOB-DTPA (gadoxetic acid, Primovist®; Schering, Berlin, Germany), with the dual functions of extracellular agents as well as hepatocyte-specific agents, were introduced to the market [19]. They can deliver both dynamic imaging and hepatobiliary phase imaging. The hepatobiliary phase of Gd-EOB-DTPA-enhanced MRI can help to differentiate small HCC from arterial-enhancing pseudolesions such as arterioportal shunts [20]. Thus, Gd-EOB-DTPA-enhanced MRI is believed to be helpful in assessing the treatment response of locoregional therapies for HCC by differentiating small residual or recurrent tumor from benign perilesional enhancement adjacent to the treated lesion. However, until now there is no evidence in the literature as to whether Gd-EOB-DTPA-enhanced MRI might be a feasible approach to assessing the treatment response of HCC.

Evaluation of the tumor response to transarterial chemoembolization

Transarterial chemoembolization (TACE) has gained wide acceptance over the past 20 years and is currently considered as the primary therapy for unresectable HCCs. In recent prospective, randomized, controlled trials [21, 22], TACE improved the rate of survival in patients with unresectable HCC compared with that achieved with the best supportive care. Despite the recently encouraging intention-to-treat studies [23], TACE is still considered as a palliative option. TACE is also used as an adjunctive therapy to liver resection or as a bridge to liver transplantation [3]. The TACE technique consists of injecting high concentrations of chemotherapeutic agents emulsified in iodinized oil, lipiodol, to the feeding vessel of the HCC. The most widely used chemotherapeutic agent is doxorubicin or a combination of cisplatin and doxorubicin.

To assess tumor response after TACE, contrast-enhanced dynamic CT or MRI including an unenhanced image, is usually performed within 4 weeks after TACE. Follow-up imaging is also a key aspect in the tumor response assessment after TACE. In general, follow-up imaging is performed every 3–4 months following the initial assessment. The distribution and degree of lipiodol uptake within an HCC as seen on unenhanced CT and the tumor enhancement noted on contrast-enhanced CT

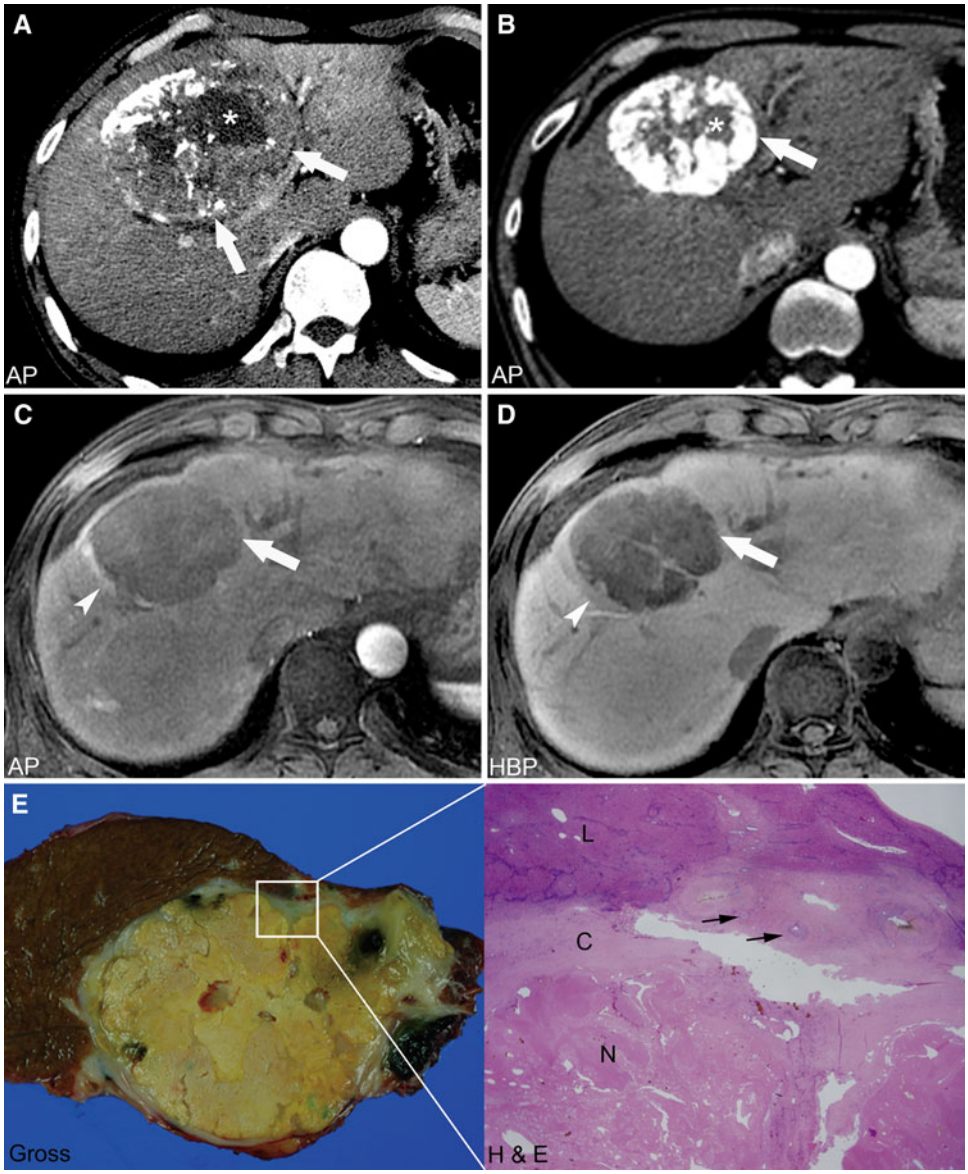

Fig. 1. Complete necrosis of HCC after transarterial chemoembolization. **A** Arterial phase of a follow-up CT obtained after the first sessions of TACE demonstrates a partially lipiodolized, large encapsulated HCC (*arrow*) in segments 4 and 8. The mass has a central, low-attenuated, necrotic portion (*asterisk*), and a peripheral solid portion. **B** On the arterial phase of a follow-up CT obtained after the fourth session of TACE, the mass shows intense deposition of lipiodol in the peripheral portion (*arrow*) and in the non-lipiodolized, central, necrotic portion (*arrowheads*). **C** Arterial phase of a Gd-EOB-DTPA-enhanced MRI after the fourth session of TACE demonstrates peritumoral rim enhancement (*arrowhead*) in the right lateral aspect of the non-enhancing, lipiodolized mass (*arrow*). **D** On the hepatobiliary phase of a Gd-EOB-DTPA-enhanced MRI, a mildly hypointense, peripheral, rim-like lesion (*arrowhead*) corresponding to the rim enhancement on MRI as seen in (**C**). The peripheral, rim-like lesion is uniform in thickness and has a smooth margin, both of which are indicative of a pseudocapsule with reactive granulation tissue. **E** Surgical gross specimen (*left*) shows a large, necrotic, encapsulated tumor with no viable portion. The *rectangle* represents the microscopic, histologic examination (Hematoxylin–Eosin stain, original magnification ×10) (*right*) which shows a fibrocollagenous pseudocapsule (*C*) with blood vessels (*arrows*) and inflammatory cells (not shown) between normal liver (*L*) and necrotic tumor (*N*).

or MRI, provide information regarding the extent of both tumor necrosis and the viable tumor portion. Enhancing portions of the tumor are presumed to be viable whereas the non-enhancing ones are presumed to be necrotic (Fig. 1). Compact lipiodol uptake is associated with prolonged median survival but does not indicate complete necrosis [24]. The lack of a satisfactory response after one session of TACE does not

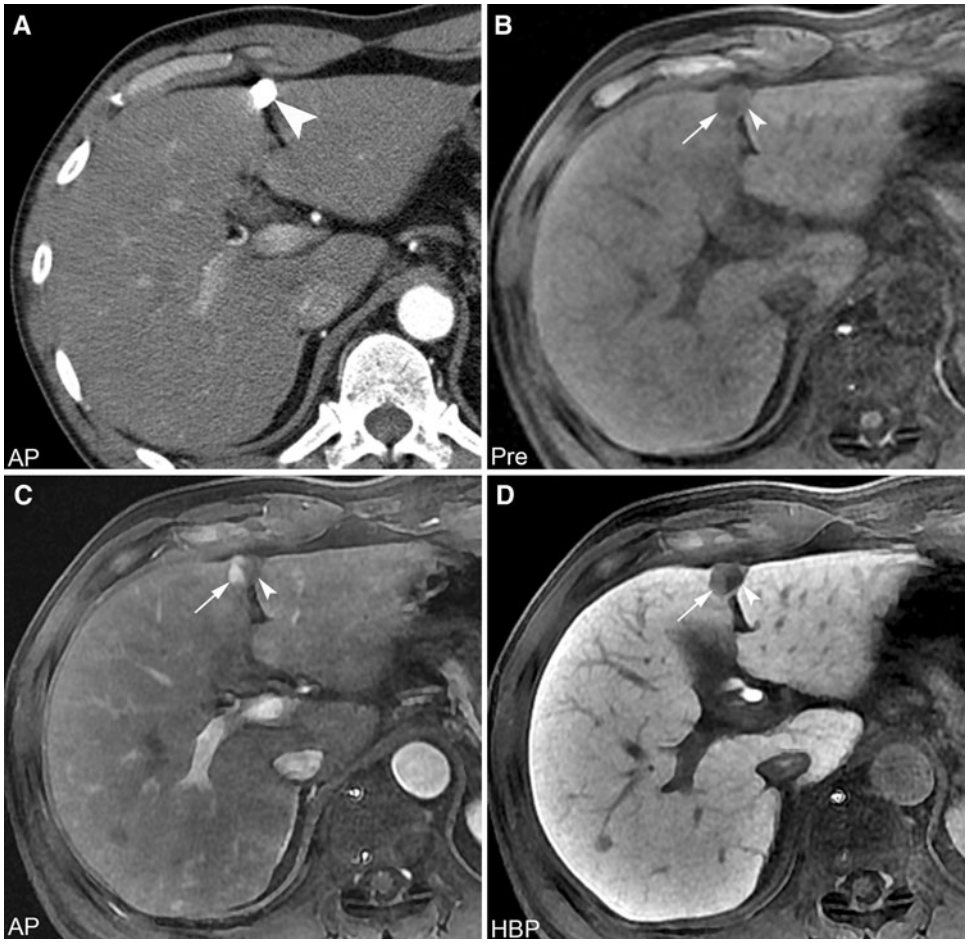

Fig. 2. Obscured viable tumor in a lipiodolized mass seen on CT. **A** An arterial phase CT image obtained 4 months after TACE shows uniform, dense deposition of lipiodol in a small tumor (*arrowhead*) in segment 4 of the liver. On the Gd-EOB-DTPA-enhanced MRI obtained 2 weeks after the CT scan obtained to assess possibly elevated alpha-fetoprotein blood level, a viable tumor portion (*arrows*) shows hypointensity on a precontrast image (**B**), strong enhancement on an arterial phase image (**C**), and moderate hypointensity on a hepatobiliary image (**D**). The necrotic portion (*arrowheads*) shows loss of contrast enhancement during all dynamic phases.

suggest the eventual tumor response, and repeated treatments targeting the same lesion must sometimes be performed.

To assess questionable areas of enhancement on CT, MR is advantageous. The high attenuation density of the lipiodol on CT scans after chemoembolization may obscure a small, enhancing, viable tumor portion within or adjacent to the lesion due to the beam-hardening artifact [25]. As the lipiodol deposition in the tumor does not affect the MR signal intensity, Gadolinium-enhanced dynamic MRI can determine areas of tumor enhancement (Fig. 2). However, with perilesional enhancement on contrast-enhanced MRI, it is still difficult to discriminate the peripheral, viable tumor portion from adjacent reactive granulation tissue or an arterio-portal shunt (Fig. 1). Contrast enhancement in granulation tissue is believed to be caused by increased capillary permeability as well as a marked increase in the passive distribution of gadolinium [26]. The equilibrium phase of dynamic MRI or the hepatobiliary phase of Gd-EOB-DTPA-enhanced MRI is frequently helpful for discerning the viable tumor portion which shows low-signal intensity on MRI due to the wash-out of contrast agent and lack of functioning hepatocyte [27]. The MR signal intensity of an HCC treated with TACE may vary. Low-signal intensity on T2-weighted images represents necrosis. Conversely, high-signal intensity on T2-weighted images corresponds to residual tumor. However, adjacent granulation tissue with inflammatory infiltration, hemorrhage or liquefied necrosis also can show high-signal intensity on T2-weighted images [13]. The recent advances in DW-MRI may be helpful for discerning the viable tumor portion which shows high-signal intensity on DW-MRI with a low ADC value from the necrotic tissue or non-tumorous liver parenchyma which shows iso- or low-signal intensity on DW-MRI with a high ADC value (Fig. 3). There have been several reports regarding the use of DW-MRI to evaluate HCC response to TACE and which show the variable diagnostic performance of DW-MRI for detecting the viable tumor portion after TACE compared with that of contrast-enhanced MRI [14, 26–29]. Therefore, DW-MRI should be validated in larger prospective studies, although we anticipate that the combined use of DW-MRI with dynamic contrast MRI is helpful in providing higher sensitivities than conventional, contrast-enhanced MRI alone for the detection of locally recurrent tumor after TACE.

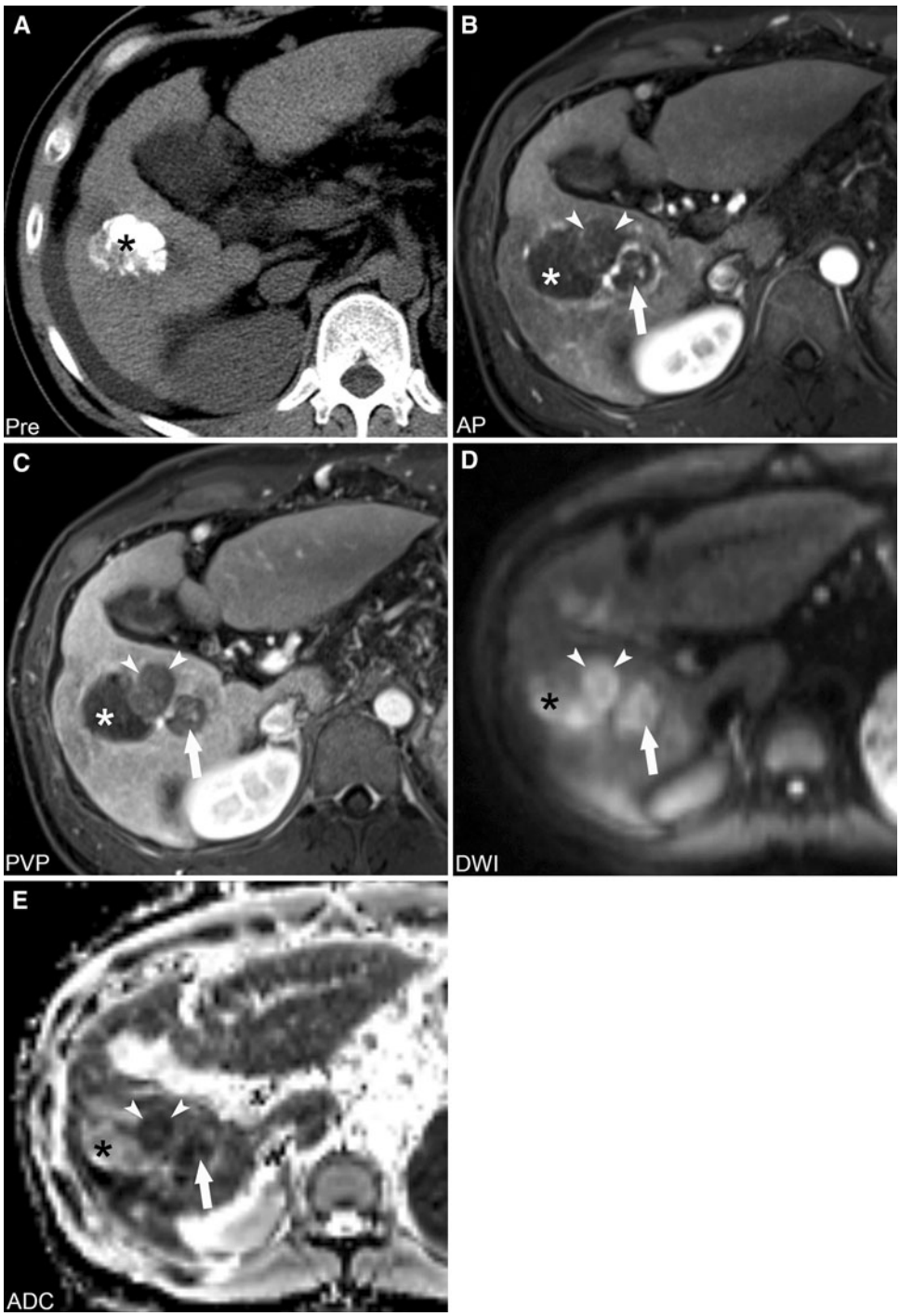

Fig. 3. Diffusion-weighted MRI for a locally recurrent tumor after TACE. **A** A precontrast CT image obtained 3 weeks after TACE shows dense accumulation of lipiodol in the HCC (*asterisk*). The arterial phase (**B**) and portal venous phase (**C**) images of Gd-EOB-DTPA-enhanced MRI obtained 3 months after TACE show two newly developed, poorly enhancing masses (*arrowheads* and *arrows*) adjacent to the lipiodolized, non-enhancing mass (*asterisks*). **D**, **E** The newly developed masses (*arrowheads* and *arrows*) demonstrate high-signal intensity on DW-MRI with a *b*-value of 500 s/mm^2 (**D**) and a low ADC value on the ADC map (**C**), thus indicating restricted diffusion of the cellular, viable tumor. The non-viable lipiodolized mass (*asterisks*) shows high-signal intensity on both DW-MRI and the ADC map, thus indicating a T2 shine-through effect of the lesion.

Evaluation of the tumor response to transarterial radioembolization

Intra-arterial brachytherapy involving the administration of Yttrium-90 microspheres selectively into the peritumoral or intratumoral arteries, is known as transarterial radioembolization. Yttrium-90 emits high-energy beta rays with a mean tissue penetration of 2.5 mm and a maximum penetration of 11 mm. As the mean energy and mean penetration of Yttrium-90 are substantial, it can be used to treat larger tumors. Intra-arterial administration of Yttrium-90-embedded microspheres can provide a higher dose of radiation to the tumor while sparing the normal liver [30]. Currently, TARE with Yttrium-90 is used to treat unresectable HCC [31].

As with TACE, imaging is essential to assess the therapeutic response of HCC after TARE [32]. There have been several criteria used to determine the tumor response to TARE with Yttrium-90, including anatomic

imaging criteria according to RECIST, WHO, or the EASL guidelines as well as functional imaging criteria using DW-MRI or PET [33]. Determination of the tumor size change is the standard measurement of the treatment response. However, the tumor necrosis and enhancement degree of the tumor seen on contrast-enhanced CT or MRI should be considered according to the recommendations of the EASL guidelines [34]. In addition, diffusion MRI has been shown to be a promising technique for evaluating early tumor response as it has an increased ADC value after TARE (Fig. 4) [35]. A recent study recommended that anatomic imaging criteria be used as the primary method to determine tumor response and that functional imaging criteria be used as a complementary secondary method [33].

Given the internal radiation effect of the Yttrium-90 microspheres, the imaging findings imparted by this mode of action of TARE differ from TACE. Local radiation effect of Yttrium-90 can lead to peripheral ring enhancement around the radioembolized tumor and perivascular edema along the portal triads that may last several months [36]. Histologically, radiation-induced liver disease is characterized by central venous congestion, erythrocyte entrapment, and atrophy of hepatocytes [30]. Without knowledge of this phenomenon, perivascular edema or ring enhancement on MRI may be incorrectly ascribed as infiltrative disease. The DW-MRI may help to distinguish enhancement due to post-treatment inflammation from viable tumor, as increased water diffusion can be demonstrated in inflammation (Fig. 4).

Fig. 4. Diffusion-weighted MRI for tumor response assessment after radioembolization. **A** The Gd-EOB-DTPA-enhanced MRI obtained before radioembolization demonstrates a large HCC (*arrowheads*) with enhancement on the arterial phase image (*left*) and marked hypointensity on the hepatobiliary phase image (*right*). **B** On the DW-MRI (*left*) and the ADC map (*right*) obtained before radioembolization, the mass (*arrowheads*) shows high-signal intensity on DW-MRI and a low ADC value, both of which are indicative of a highly cellular tumor. **C** Gd-EOB-DTPA-enhanced MRI obtained 2 months after radioembolization with Yttirium-90 reveals the amount of tumor decrease as well as necrosis of the central tumor portion (*asterisk*). An arterial phase MR image (*left*) reveals peripheral rim enhancement (*arrowheads*) and an irregularly enhancing, nodular lesion (*arrow*). On an hepatobiliary phase image (*right*), the hypointense, rim-like lesion (*arrowheads*) around the tumor as well as a hypointense, nodular portion (*arrow*) in the posterolateral aspect of the tumor were noted and thus raise the suspicion of there being a viable tumor. **D** The DW-MRI (*left*) and the ADC map (*right*) obtained 2 months after radioembolization show that the ADC value of the tumor markedly increased compared to that seen in (**B**). The signal intensity of the tumor on DW-MRI also increased due to the T2 shine-through effect of the T2, hyperintense, necrotic tumor portion. The nodular portion (*arrow*) in the posterolateral aspect of the tumor still shows a low ADC value with high-signal intensity on DW-MRI, thus indicating viable tumor. **E** The surgical gross specimen (*left*) shows a large necrotic tumor with a viable nodular portion (*rectangle*) and extensive congestion in the adjacent parenchyma (*arrowheads*). The *rectangle* represents the microscopic, histologic examination (Hematoxylin–Eosin stain, original magnification ×10) (*right*) which showed the necrotic portion (N) with Yttrium-90 microspheres (*arrow*), extensive red blood cell congestion (C) in the peripheral portion of the tumor, as well as a viable tumor portion (T).

Evaluation of the tumor response to RF ablation

Radiofrequency ablation is the most widely used thermal ablation therapy for both resectable and unresectable HCC. Alternating electric current in the RF range of 200–1200 kHz is used to produce local ionic agitation and subsequent frictional heat in the tissue surrounding the RF electrode, which then produce coagulation necrosis [37]. Imaging has a crucial role in the follow-up of HCC treated with RF ablation as it is the means by which the local treatment efficacy, recurrent disease, and some therapy-induced complications are evaluated. Basically, the assessment of RF ablation of HCC can be made by contrast-enhanced CT or MRI to evaluate a non-enhancing necrotic ablation zone and an enhancing viable tumor. The non-enhancing ablation zone should exceed the tumor margins by 0.5–1 cm [38]. The area of RF-induced coagulation necrosis area usually involutes with time, although most often very slowly (Fig. 5). In a recent study, the mean percentages of volume change at 1, 4, 10, 16, and 19 months were 79%, 50%, 27%, 11%, and 6%, respectively, compared with the volume seen on immediate follow-up CT [39]. Therefore, size criteria such as those of the WHO and RECIST guidelines cannot be used to assess the tumor response to RF ablation therapy. Serial follow-up imaging is usually the most valuable method for treatment response assessment of RF ablation [40].

The protocol for the frequency and length of imaging follow-up after RF ablation is not well established [41]. In many institutions, including our hospital, immediate post-procedure imaging is performed to evaluate the presence of residual tumor and a sufficient ablative margin, so that another session of ablation can be performed if the ablation does not achieve technical success. Assessment of immediate complications such as hemorrhage, major vessel injury, pneumothorax, or adjacent organ injury, is also an important function of the immediate post-procedure imaging. However, immediate imaging is not universally recommended as the evaluation is confused by the presence of any benign periablational enhancement surrounding the ablation zone and that may obscure viable tumor [36]. The benign periablational enhancement is resolved by the 1-month

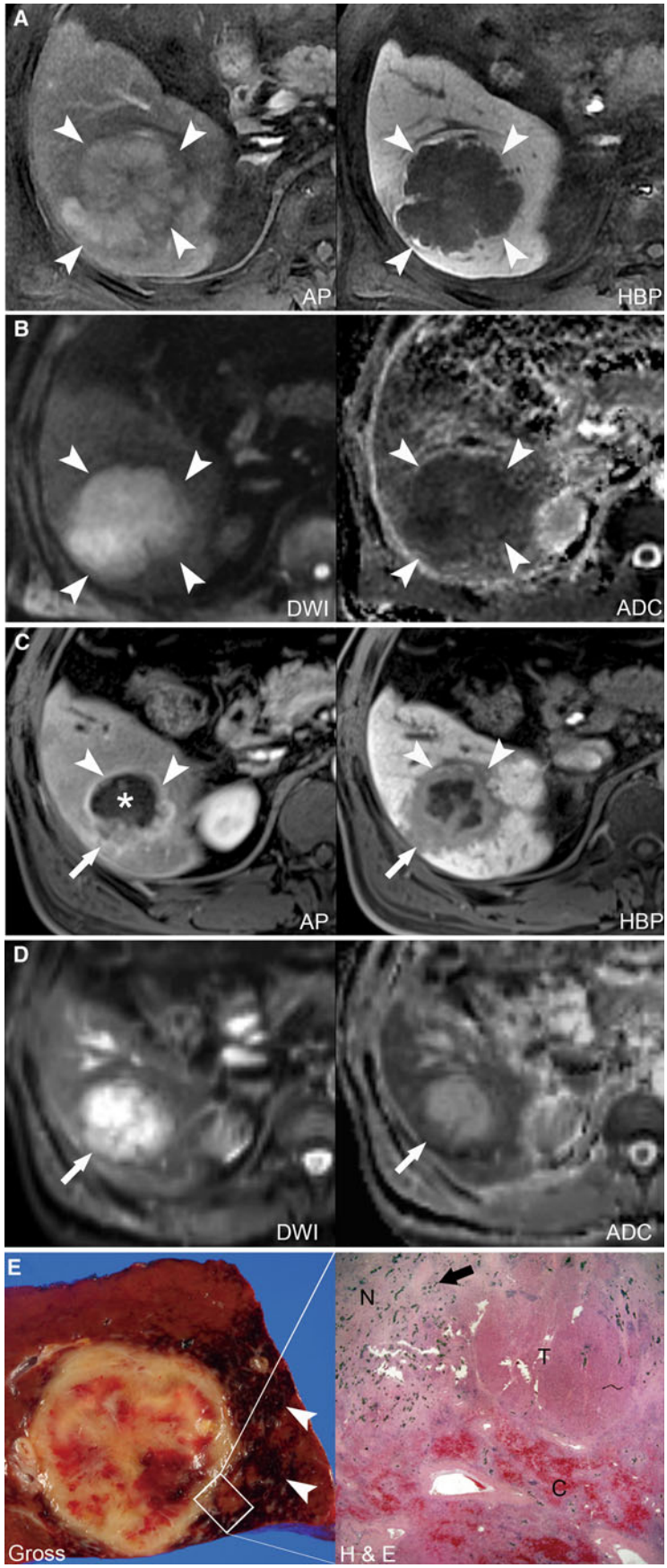
A
AP
HBP
B
DWI
ADC
C
AP
HBP
D
DWI
ADC
E
Gross
N
T
C
H & E

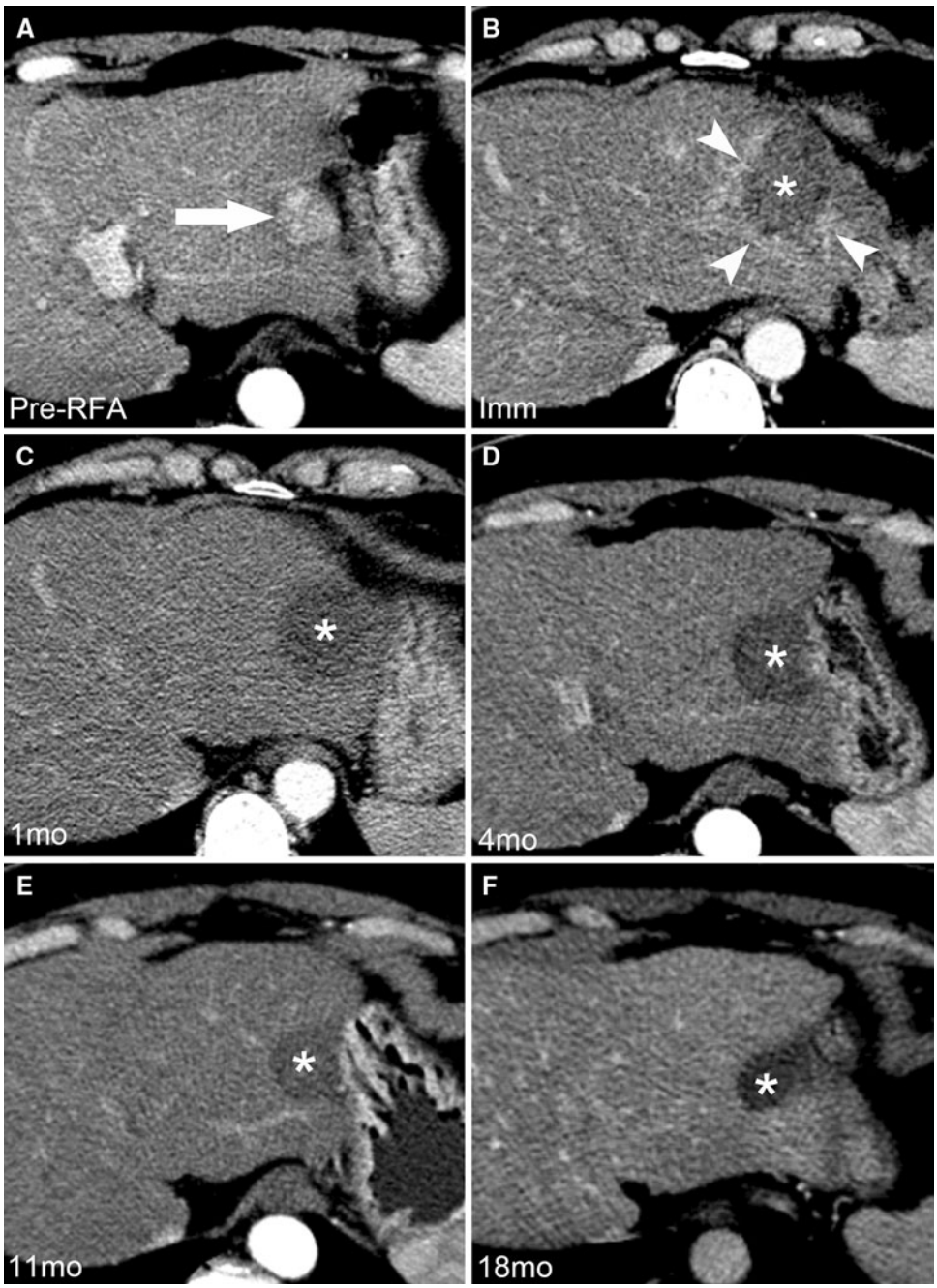

Fig. 5. Gradual involution of the ablation zone after RF ablation. **A** On an arterial phase CT image obtained before RF ablation, an enhancing nodule (*arrow*) is noted in the left lateral segment of the liver. **B** An arterial phase CT image obtained immediately after RF ablation shows an ablation zone (*asterisk*) with loss of contrast enhancement. Note the uniform peripheral enhancement (*arrowheads*) which is only seen on immediate post-ablation CT and is indicative of benign, periablational enhancement. **C**–**F** Serial follow-up CT images of the RF ablation demonstrate the gradual decrease in the size of the ablation zone (*asterisks*).

follow-up CT in most patients [39]. One-month follow-up CT or MRI is essential in order to detect local tumor progression when it is smallest in size. Subsequent serial contrast-enhanced CT or MR every 3 months for at least 1 year and every 6 months thereafter is the widely used imaging protocol for follow-up of treated patients [36].

In the early post-ablation period, the ablation zone typically appears as a non-enhancing area of low attenuation or low-signal intensity on contrast-enhanced CT or MRI. On CT, the ablation zone often contains a central area of high attenuation along the electrode needle tract; this has usually disappeared by the next follow-up CT [42]. On MRI, the ablation zone shows variable signal intensity (Fig. 6). T1-signal intensity is determined by the stage of the hemorrhage, whereas T2-signal intensity depends on the presence of coagulation necrosis or liquefactive necrosis. The ablation zone where coagulation necrosis occurs typically show T2-hypointensity, whereas areas of liquefactive necrosis or a fluid cavity in the ablation zone shows T2-hyperintensity. Although viable tumor shows T2-hyperintensity, it may be masked by the heterogenous T2-signal intensity of the ablation zone. Therefore, contrast-enhanced MRI should

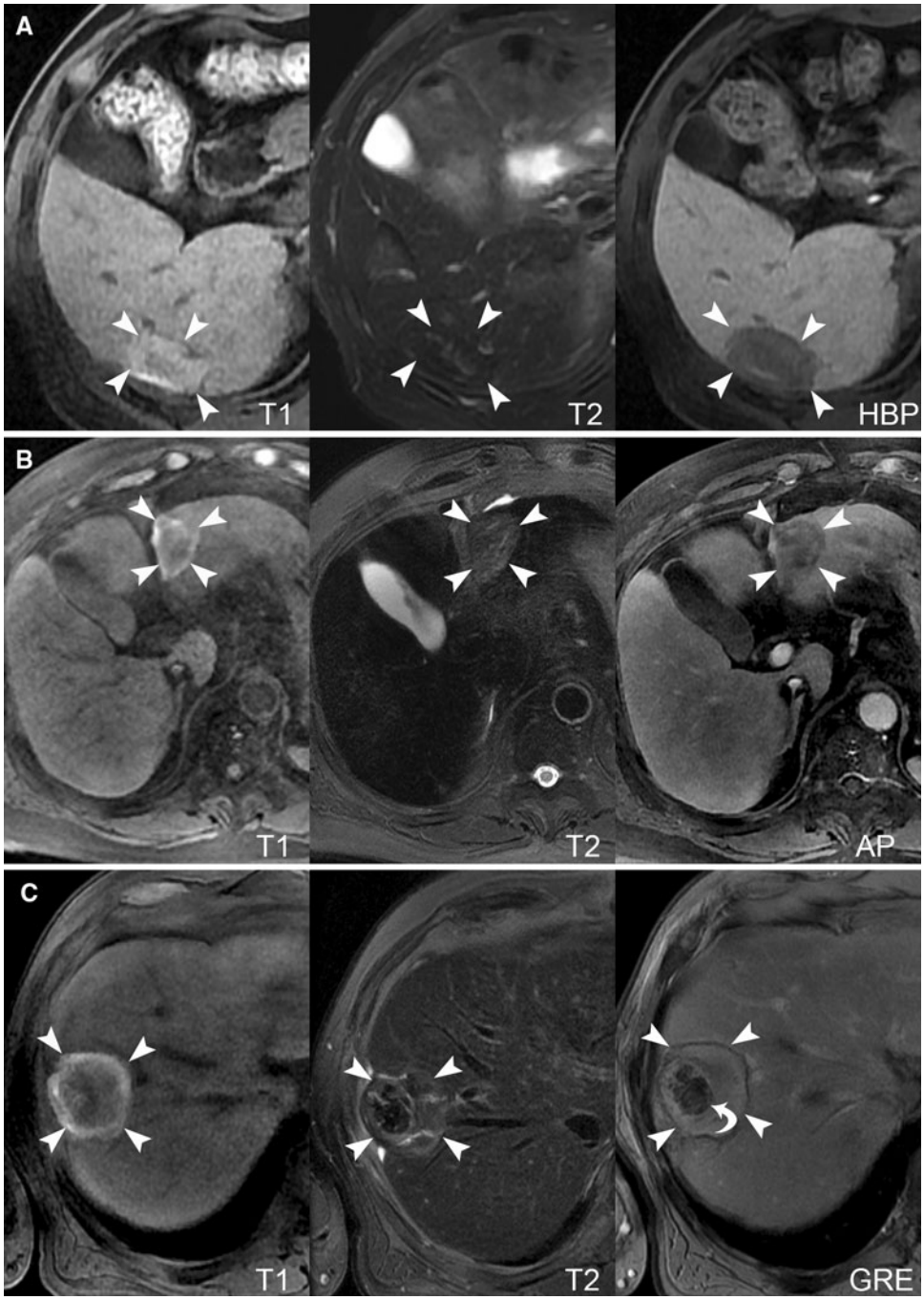

Fig. 6. Variable signal intensity of the RF ablation zone as seen on MR. **A** On a Gd-EOB-DTPA-enhanced MRI obtained 1 year after RF ablation, the ablation zone (*arrowheads*) shows hyperintensity on T1-weighted MRI (*left*), isointensity on T2-weighted MRI (*middle*), and marked hypointensity on the hepatobiliary phase (*right*). **B** On a Gd-EOB-DTPA-enhanced MRI obtained 1 year after RF ablation, the ablation zone (*arrowheads*) shows peripheral hyperintensity and central hypointensity on T1-weighted MRI (*left*), homogenous hyperintensity on T2-weighted MRI (*middle*), and loss of enhancement on arterial phase imaging (*right*). **C** On a Gd-EOB-DTPA-enhanced MRI obtained 10 months after RF ablation, the ablation zone (*arrowheads*) shows peripheral hyperintensity and central hypointensity on T1-weighted MRI (*left*) and heterogenous signal intensity on T2-weighted MRI (*middle*). On a T2-weighting gradient echo image (*right*), the hemorrhagic portion is shown as dark signal intensity (*curved arrow*) in the tumor.

be performed for accurate treatment assessment after ablation [43].

As mentioned, benign periablational enhancement surrounding the ablation zone is frequently found to show moderate to intense peripheral rim-like enhancement on the arterial phase of contrast-enhanced CT or MRI. It usually is shown as iso-attenuation on the delayed phase of CT, but may show persistent enhancement on the delayed phase of MRI. This rim has low-signal intensity on T1-, and high-signal intensity on T2-weighted images. Histologic analysis of the perilesional rim has revealed that it is initially reactive hyperemia and subsequently fibrosis and a giant cell reaction [38, 40, 41]. This peripheral rim most often measures 1–2 mm, but can measure up to 5 mm, and regresses progressively (Fig. 7). Lim et al. reported that periablational enhancement was noted on CT in 79% of their patients and had disappeared by 1 month after ablation in all patients [39], although it may last for up to 6 months [41]. It is a relatively concentric, symmetric, and uniform process with smooth inner margins, and it should be differentiated from irregular peripheral enhancement which may indicate incomplete local treatment.

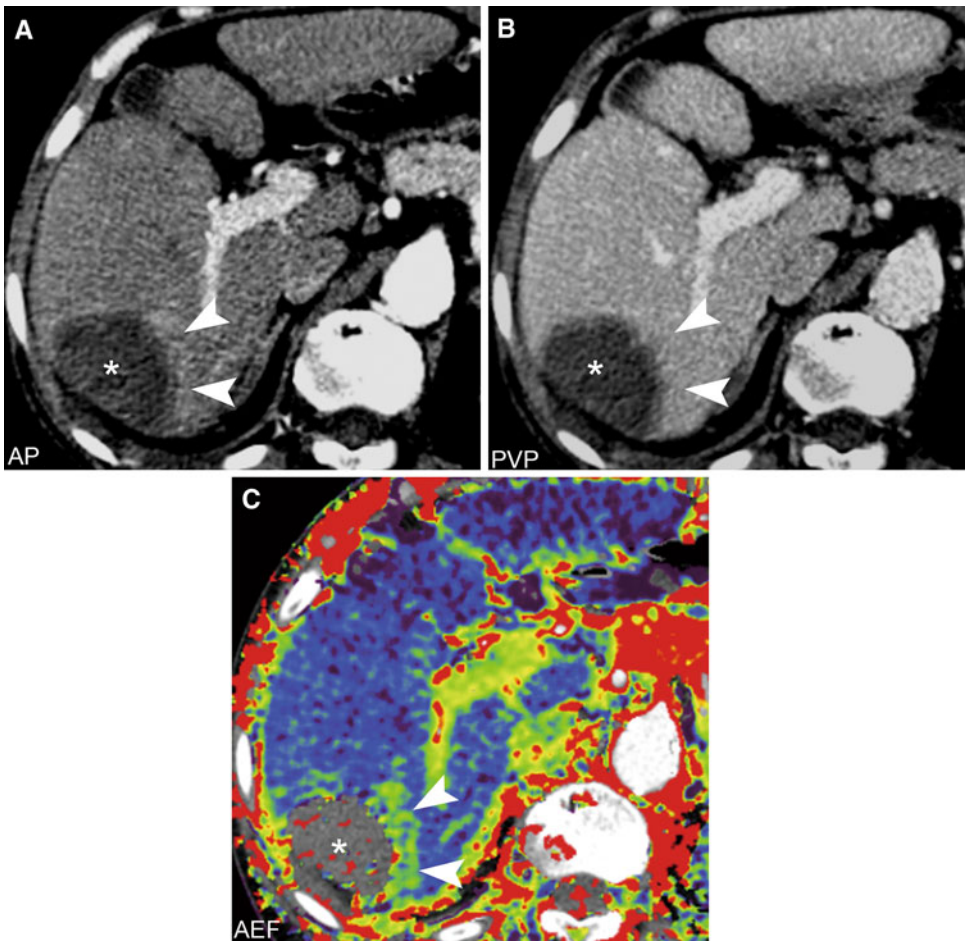

Fig. 7. Benign periablational enhancement after RF ablation. **A** On an arterial phase CT image obtained 1 month after RF ablation, thick, uniform, peripheral enhancement (*arrowheads*) was noted at the medial aspect of the ablation zone (*asterisk*). **B** On a portal venous phase CT image, the peripheral enhancement becomes iso-attenuated and indistinguishable from normal liver parenchyma (*arrowheads*), which is indicative of benign periablational enhancement. **C** On color mapping of the arterial enhancement fraction (AEF), the peripheral enhancement more clearly appears as a *green-colored* lesion (*arrowheads*) with a moderately high AEF value [18]. The ablation zone appears as a *gray-colored* lesion (*asterisk*).

Needle puncture or thermal damage may result in an arterioportal shunt represented by a wedge-shaped enhancement of the liver parenchyma on the arterial phase that appears as iso-attenuation or iso-signal intensity on the equilibrium phase of contrast-enhanced CT or MRI. Most of these procedure-related arterioportal shunt lesions disappeared within 1–3 months after ablation [44].

On immediate follow-up CT, intralesional air bubbles which were small in size and number may be found and disappear by the 1-month follow-up CT. It is believed that in such cases air without an air-fluid level may have been introduced along the insertion path of the needle or may have resulted from tissue necrosis [39]. If these patients have clinical symptoms such as persistent fever for more than 2 weeks, hepatic abscess should be kept in mind as a possible cause of the fever. The increased extent of air and peripheral enhancing rims in a characteristic layering pattern seen on follow-up CT may be a sign of formation of an hepatic abscess [42] (Fig. 8).

Follow-up contrast-enhanced CT or MRI is essential for the evaluation of local tumor progression which is the preferred term to local recurrence because it is virtually impossible to determine whether there was an incompletely treated but viable tumor that continued to grow or if a new tumor grew at the original site [41]. Local tumor progression has been divided into three types: (1) the halo type which appears as an irregular, thick rim of enhancement around the ablation zone; (2) nodular type which appears as nodular foci of enhancement at the periphery of the ablation zone; and (3) gross enlargement type which is associated with an overall increase in the ablation zone [44, 45]. In HCC, the nodular and halo types occur more frequently than the gross enlargement type [36] (Fig. 9).

In a recent study regarding the respiratory-triggered DW-MRI and ADC values for follow-up after RF ablation, ADC-based evaluation of signal alterations adjacent to the ablation zone may contribute to the identification of local tumor progression and non-tumoral post-treatment tissue changes [46]. Local tumor progression lesions typically exhibit hyperintense areas in the periphery of the ablation zone on DW-MRI with low ADC values in the corresponding hyperintense areas (Fig. 10). ADC maps could, therefore, be helpful for analyzing unclear hyperintense areas adja-

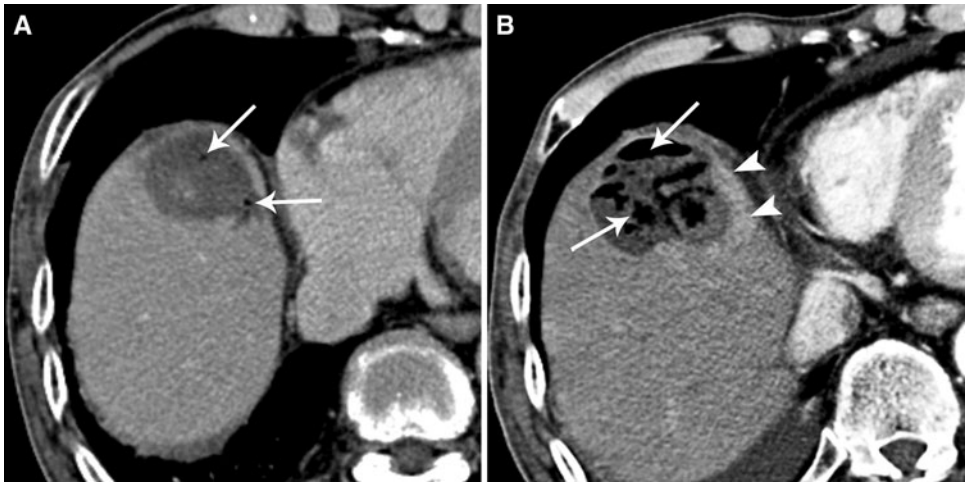

Fig. 8. Air bubbles in the RF ablation zone. **A** An immediate post-ablation CT image reveals tiny air bubbles (*arrows*) in the ablation zone, which are thought to be introduced along the insertion path of the needle. **B** On an arterial phase CT image obtained 2 weeks after RF ablation and to evaluate persistent fever, the amount of air (*arrows*) in the ablation zone and the extent of the peripheral enhancing rim (*arrowheads*) have increased, thus indicating findings of hepatic abscess.

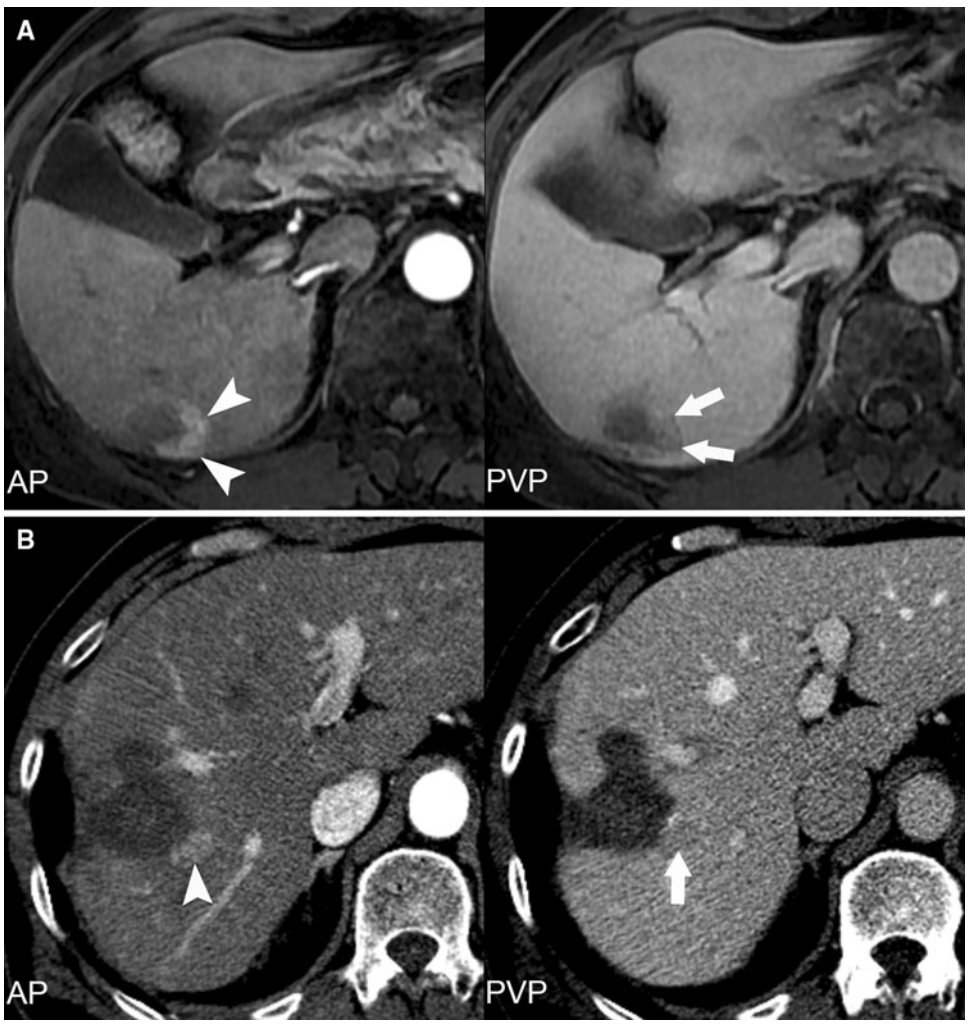

Fig. 9. Types of local tumor progression of HCC after RF ablation. **A** Halo type. Arterial phase image (*left*) of Gd-EOB-DTPA-enhanced MRI obtained 1 year after RF ablation demonstrates a newly developed, thick, irregularly enhancing rim (*arrowheads*) at the medial aspect of the non-enhancing ablation zone, and which becomes a hypointense lesion (*arrows*) due to wash-out of contrast agent on the portal venous phase (*right*). **B** Nodular type. On CT images obtained 6 months after RF ablation, a newly developed nodule is seen at the medial aspect of the ablation zone and shows arterial enhancement (*arrowhead*) on the arterial phase image (*left*) and portal wash-out (*arrow*) on the portal phase image (*right*).

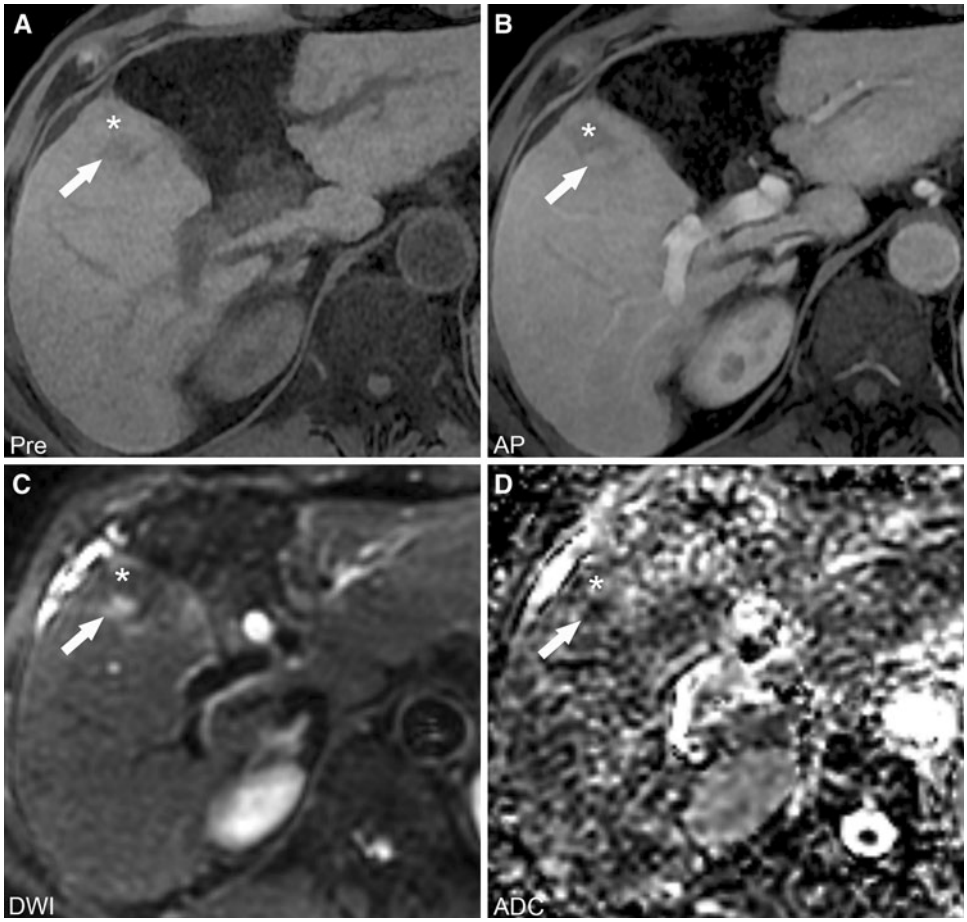

Fig. 10. Diffusion-weighted MRI to evaluate RF ablation. **A** On a precontrast, T1-weighted MR image obtained 18 months after RF ablation, there is a newly developed hypointense nodule (*arrow*) at the posterior aspect of the ablation zone (*asterisk*); this is indicative of local tumor progression after RF ablation. **B** An arterial phase, Gd-EOB-DTPA-enhanced MR image shows arterial enhancement of the nodule (*arrow*) and loss of enhancement in the ablation zone (*asterisk*). **C** On DW-MRI with a *b*-value of 100 s/mm^2, the nodule (*arrow*) shows high-signal intensity and the necrotic ablation zone (*asterisk*) shows low-signal intensity. **D** On the ADC map, the nodule (*arrow*) shows a low ADC value while the ablation zone (*asterisk*) has a high ADC value. The hyperintensity of the nodule seen on DW-MRI with a low ADC value is presumed to represent the water diffusion restriction of the cellular viable tumor.

cent to the ablation zone where differentiation between tumor tissue and post-treatment changes is unambiguous. It has been demonstrated that unclear signal alterations in the periphery of the ablation zone exhibited markedly lower ADC values in patients with local tumor progression on follow-up DW-MRI and in the ADC map.

In a recent study regarding follow-up imaging of fatty HCC lesions after RF ablation, persistent fat content was observed on follow-up imaging in all post-ablation lesions. The persistence of fat did not necessarily indicate treatment failure, although an increase or decrease in the fat content (increase or decrease in size) can be used as an additional criterion for the determination of treatment success [47].

Evaluation of the treatment response to ethanol ablation

Ethanol ablation is the preferred term to percutaenous ethanol injection (PEI). The term ''instillation'' for the direct delivery of pharmacologic agents is preferred to injection, given that many pharmaceutical agents are able to be injected [41]. Ethanol ablation induces coagulation necrosis of a tumor by introducing a needle into the lesion followed by slow instillation of ethanol. Ethanol ablation is effective in the treatment of small, localized HCC in patients not eligible for surgery. The low rate of procedure-related complications and the low cost of ethanol ablation are additional advantages of its use. The main drawback of this technique is the need for repeated instillation in

separate sessions due to the high tumor recurrence rate (up to 50 by 2 years) [3]. There has been a recent shift from the use of ethanol ablation to RF ablation. In a recent systemic review, RF ablation demonstrated a significantly improved 3-year survival rate in HCC patients, compared with that of ethanol ablation [48].

There are many similarities between the radiologic aspect of RF-induced destruction and the necrosis induced by ethanol [49]. The coagulation necrosis area typically shows T1-hyperintensity and T2-hypointensity, and the viable tumor shows T2-hyperintensity in both the RF ablation zone and the ethanol ablation zone. However, liquefactive necrosis can also cause T2-hyperintensity which can limit the T2-weighted signal intensity pattern of tumors injected with alcohol to ascertain tumor viability [43, 49]. Therefore, contrast-enhanced MRI or CT is more reliable for evaluating treatment effectiveness. Local tumor progression usually manifests as a tumor around the ablation zone and in continuity with its border (outgrowth) or as an enhancing lesion within the edge of the necrotic ablation zone (ingrowth) (Fig. 11).

The difference between the RF ablation zone and the ethanol ablation zone is that the area of RF-induced coagulation necrosis shrinks more slowly than that of ethanol-induced necrosis. Ebara et al. reported shrinkage of all of the ethanol ablation zone which attained a mean size of 45% at 6 months and 63% at 12 months in 67 HCCs treated with ethanol [50].

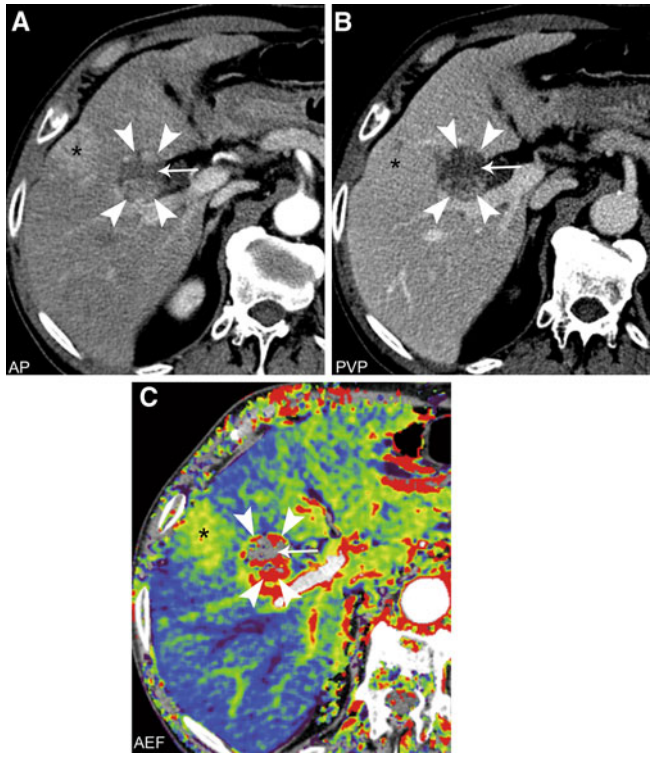

Fig. 11. Local tumor progression after ethanol ablation. **A** The arterial phase, 6-month follow-up CT image obtained after ethanol ablation shows newly developed, arterial-enhancing lesions (*arrowheads*) within the ablation zone (*arrow*); this is indicative of the ingrowth pattern of local tumor progression. Note the peripheral geographic, high-attenuated lesion around the needle track in the liver parenchyma (*asterisk*). This is depicted only on the arterial phase image and is indicative of the procedure-related arterioportal shunt. **B** On the portal venous phase image, the enhancing lesion (*arrowheads*) within the ablation zone (*arrow*) shows washout of the contrast agent. **C** Color mapping of the AEF shows red-colored, recurrent tumor (*arrowheads*) in the *gray-colored* RF ablation zone (*arrow*).

Evaluation of the tumor response to targeted therapy

Although conventional systemic chemotherapy has not been effective treatment for HCC, recent advances in targeted therapy present a promising new therapeutic option. Sorafenib, which is an oral multikinase inhibitor, blocks tumor cell proliferation and exerts an anti-angiogenic effect within the tumor. A recent phase III randomized trial referred to as the SHARP trial (Sorafenib HCC Assessment Randomized Protocol), indicates that sorafenib significantly improves patient survival and doubles the time to tumor progression among patients with advanced HCC [51].

The main effect of sorafenib for HCC treatment is disease stabilization rather than a direct cytotoxic effect accompanied by tumor shrinkage. Therefore, morphologic tumor changes do not constitute appropriate criteria for the therapeutic response assessment. Sorafenib is expected to reduce tumor vascularization and to subsequently induce tumor necrosis and hemorrhage. In a recent study, the temporary expansion of HCC during sorafenib therapy was noted in more than one-third of the tumors; this is believed to be caused primarily by the increased tumor volume induced by tumor necrosis [52]. Therefore, the traditional tumor response assessment criteria such as WHO, RECIST or the EASL guidelines, are not reliable when assessing new, targeted therapies.

The focus of response monitoring of this novel therapeutic agent should include the assessment of these parameters such as reduced vascularity, induced necrosis, and hemorrhage in the tumor. On contrast-enhanced CT, the enhancement degree of HCC may decrease during sorafenib therapy (Fig. 12). However, the enhancement degree of the tumor depends on the CT scan protocol, contrast agent injection protocol and patient cardiovascular status at the time of scanning. Perfusion CT and its perfusion parameters may allow a more accurate quantification of the tumor perfusion [53]. On MRI, the T1 and T2-signal intensity varies according to the presence of hemorrhage and necrosis. Contrast-enhanced MRI

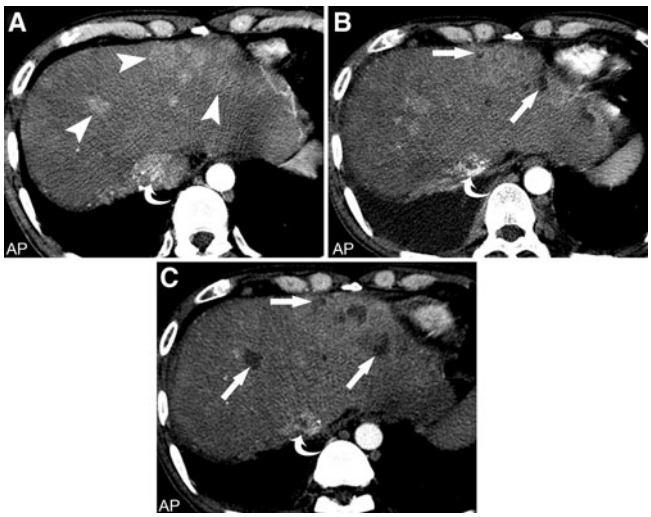

Fig. 12. A 66-year-old man who had been treated with sorafenib for an unresectable HCC. **A** An arterial phase CT image in the baseline setting reveals multiple, arterial-enhancing masses (*arrowheads*) in both liver lobes. Note the bulky, enhancing tumor thrombosis in the IVC (*curved arrow*). **B** A follow-up CT image obtained 1 month after the beginning of sorafenib therapy reveals that the extent of the enhancing mass has not changed, but that there are multifocal, small, necrotic foci (*arrows*) within the enhancing masses. **C** A follow-up CT image obtained 1 month after (**B**) reveals increase in the extent of the multiple necrotic lesions (*arrows*) in the enhancing masses. The enhancing masses and the tumor thrombosis (*curved arrow*) in the IVC show a further decrease in size.

can also show the reduction in tumor perfusion. These specific responses of HCC to sorafenib therapy also allow early differentiation between responder and non-responder.

Conclusion

Unlike treatment of other oncologic tumors, locoregional treatment and transarterial therapies are mainstay treatments of HCC. Treatment response assessment using imaging is a key factor in the management of patients with HCC. The application of classical WHO or RECIST criteria may not be suitable for accurate treatment response assessment of locoregional treatment or targeted therapy for HCC. Therefore, an understanding of the imaging features of post-treatment imaging after various treatment modalities for HCC is crucial for treatment response assessment and for determining further therapy.

Acknowledgments. We thank Bonnie Hami, M.A. for her editorial assistance. This work was partly supported by Basic Science Research Program through the National Research Foundation of Korea (NRF) (Grant No. 800-20100430).

References

1. Lau WY, Lai EC (2008) Hepatocellular carcinoma: current management and recent advances. Hepatobiliary Pancreat Dis Int 7:237–257
2. Sauer P, Kraus TW, Schemmer P, et al. (2005) Liver transplantation for hepatocellular carcinoma: is there evidence for expanding the selection criteria? Transplantation 80:S105–S108
3. Rampone B, Schiavone B, Martino A, Viviano C, Confuorto G (2009) Current management strategy of hepatocellular carcinoma. World J Gastroenterol 15:3210–3216
4. Lau WY (1997) The history of liver surgery. J R Coll Surg Edinb 42:303–309
5. Zhang T, Ding X, Wei D, et al. (2010) Sorafenib improves the survival of patients with advanced hepatocellular carcinoma: a meta-analysis of randomized trials. Anticancer Drugs 21:326–332
6. World Health Organization (WHO) (1979) *WHO Handbook for Reporting Results of Cancer Treatment*. Geneva, Switzerland: WHO. WHO Offset Publication No. 48
7. Therasse P, Arbuck SG, Eisenhauer EA, et al. (2000) New guidelines to evaluate the response to treatment in solid tumors. European Organization for Research and Treatment of Cancer, National Cancer Institute of the United States, National Cancer Institute of Canada. J Natl Cancer Inst 92:205–216
8. Eisenhauer EA, Therasse P, Bogaerts J, et al. (2009) New response evaluation criteria in solid tumours: revised RECIST guideline (version 1.1). Eur J Cancer 45:228–247
9. Riaz A, Miller FH, Kulik LM, et al. (2010) Imaging response in the primary index lesion and clinical outcomes following transarterial locoregional therapy for hepatocellular carcinoma. JAMA 303: 1062–1069
10. Forner A, Ayuso C, Varela M, et al. (2009) Evaluation of tumor response after locoregional therapies in hepatocellular carcinoma: are response evaluation criteria in solid tumors reliable? Cancer 115:616–623
11. Bruix J, Sherman M, Llovet JM, et al. (2001) Clinical management of hepatocellular carcinoma. Conclusions of the Barcelona-2000 EASL conference. European Association for the Study of the Liver. J Hepatol 35:421–430
12. Harry VN, Semple SI, Parkin DE, Gilbert FJ (2010) Use of new imaging techniques to predict tumour response to therapy. Lancet Oncol 11:92–102
13. Vossen JA, Buijs M, Kamel IR (2006) Assessment of tumor response on MR imaging after locoregional therapy. Tech Vasc Interv Radiol 9:125–132
14. Yu JS, Kim JH, Chung JJ, Kim KW (2009) Added value of diffusion-weighted imaging in the MRI assessment of perilesional tumor recurrence after chemoembolization of hepatocellular carcinomas. J Magn Reson Imaging 30:153–160
15. Youn BJ, Chung JW, Son KR, et al. (2008) Diffusion-weighted MR: therapeutic evaluation after chemoembolization of VX-2 carcinoma implanted in rabbit liver. Acad Radiol 15:593–600
16. Chen G, Ma DQ, He W, Zhang BF, Zhao LQ (2008) Computed tomography perfusion in evaluating the therapeutic effect of transarterial chemoembolization for hepatocellular carcinoma. World J Gastroenterol 14:5738–5743
17. Jackson A, Haroon H, Zhu XP, et al. (2002) Breath-hold perfusion and permeability mapping of hepatic malignancies using magnetic resonance imaging and a first-pass leakage profile model. NMR Biomed 15:164–173
18. Kim KW, Lee JM, Klotz E, et al. (2009) Quantitative CT color mapping of the arterial enhancement fraction of the liver to detect hepatocellular carcinoma. Radiology 250:425–434
19. Choi BI, Lee JM (2009) Advancement in HCC imaging: diagnosis, staging and treatment efficacy assessments: imaging diagnosis and staging of hepatocellular carcinoma. J Hepatobiliary Pancreat Sci 17:369–373
20. Sun HY, Lee JM, Shin CI, et al. (2010) Gadoxetic acid-enhanced magnetic resonance imaging for differentiating small hepatocellular carcinomas (< or = 2 cm in diameter) from arterial enhancing pseudolesions: special emphasis on hepatobiliary phase imaging. Invest Radiol 45:96–103
21. Llovet JM, Real MI, Montana X, et al. (2002) Arterial embolisation or chemoembolisation versus symptomatic treatment in pa-

tients with unresectable hepatocellular carcinoma: a randomised controlled trial. Lancet 359:1734–1739
22. Lo CM, Ngan H, Tso WK, et al. (2002) Randomized controlled trial of transarterial lipiodol chemoembolization for unresectable hepatocellular carcinoma. Hepatology 35:1164–1171
23. Lee HS, Kim KM, Yoon JH, et al. (2002) Therapeutic efficacy of transcatheter arterial chemoembolization as compared with hepatic resection in hepatocellular carcinoma patients with compensated liver function in a hepatitis B virus-endemic area: a prospective cohort study. J Clin Oncol 20:4459–4465
24. Riaz A, Lewandowski RJ, Kulik L, et al. (2010) Radiologic-pathologic correlation of hepatocellular carcinoma treated with chemoembolization. Cardiovasc Intervent Radiol 33:1143–1152
25. Jang KM, Choi D, Lim HK, et al. (2005) Depiction of viable tumor in hepatocellular carcinoma treated with transarterial chemoembolization: multiphasic helical CT with review of the previous serial CT images. Korean J Radiol 6:153–160
26. Kamel IR, Bluemke DA, Eng J, et al. (2006) The role of functional MR imaging in the assessment of tumor response after chemoembolization in patients with hepatocellular carcinoma. J Vasc Interv Radiol 17:505–512
27. Schima W, Ba-Ssalamah A, Kurtaran A, Schindl M, Gruenberger T (2007) Post-treatment imaging of liver tumours. Cancer Imaging 7 Spec No A:S28–S36
28. Kamel IR, Bluemke DA, Ramsey D, et al. (2003) Role of diffusion-weighted imaging in estimating tumor necrosis after chemoembolization of hepatocellular carcinoma. AJR Am J Roentgenol 181:708–710
29. Goshima S, Kanematsu M, Kondo H, et al. (2008) Evaluating local hepatocellular carcinoma recurrence post-transcatheter arterial chemoembolization: is diffusion-weighted MRI reliable as an indicator? J Magn Reson Imaging 27:834–839
30. Ibrahim SM, Nikolaidis P, Miller FH, et al. (2009) Radiologic findings following Y90 radioembolization for primary liver malignancies. Abdom Imaging 34:566–581
31. Gates VL, Atassi B, Lewandowski RJ, et al. (2007) Radioembolization with Yttrium-90 microspheres: review of an emerging treatment for liver tumors. Future Oncol 3:73–81
32. Atassi B, Bangash AK, Bahrani A, et al. (2008) Multimodality imaging following 90Y radioembolization: a comprehensive review and pictorial essay. Radiographics 28:81–99
33. Duke E, Deng J, Ibrahim SM, et al. (2010) Agreement between competing imaging measures of response of hepatocellular carcinoma to yttrium-90 radioembolization. J Vasc Interv Radiol 21:515–521
34. Salem R, Lewandowski RJ, Mulcahy MF, et al. (2010) Radioembolization for hepatocellular carcinoma using Yttrium-90 microspheres: a comprehensive report of long-term outcomes. Gastroenterology 138:52–64
35. Rhee TK, Naik NK, Deng J, et al. (2008) Tumor response after yttrium-90 radioembolization for hepatocellular carcinoma: comparison of diffusion-weighted functional MR imaging with anatomic MR imaging. J Vasc Interv Radiol 19:1180–1186
36. Gervais DA, Kalva S, Thabet A (2009) Percutaneous image-guided therapy of intra-abdominal malignancy: imaging evaluation of treatment response. Abdom Imaging 34:593–609
37. Rhim H, Goldberg SN, Dodd GD III, et al. (2001) Essential techniques for successful radio-frequency thermal ablation of malignant hepatic tumors. Radiographics 21 Spec No:S17–S35; discussion S36–S19
38. Goldberg SN, Gazelle GS, Compton CC, Mueller PR, Tanabe KK (2000) Treatment of intrahepatic malignancy with radiofrequency ablation: radiologic-pathologic correlation. Cancer 88:2452–2463
39. Lim HK, Choi D, Lee WJ, et al. (2001) Hepatocellular carcinoma treated with percutaneous radio-frequency ablation: evaluation with follow-up multiphase helical CT. Radiology 221:447–454
40. Dromain C, de Baere T, Elias D, et al. (2002) Hepatic tumors treated with percutaneous radio-frequency ablation: CT and MR imaging follow-up. Radiology 223:255–262
41. Goldberg SN, Grassi CJ, Cardella JF, et al. (2009) Image-guided tumor ablation: standardization of terminology and reporting criteria. J Vasc Interv Radiol 20:S377–S390
42. Park MH, Rhim H, Kim YS, et al. (2008) Spectrum of CT findings after radiofrequency ablation of hepatic tumors. Radiographics 28:379–390; discussion 390–372
43. Ozkavukcu E, Haliloglu N, Erden A (2009) Post-treatment MRI findings of hepatocellular carcinoma. Diagn Interv Radiol 15:111–120
44. Chopra S, Dodd GD III, Chintapalli KN, et al. (2001) Tumor recurrence after radiofrequency thermal ablation of hepatic tumors: spectrum of findings on dual-phase contrast-enhanced CT. AJR Am J Roentgenol 177:381–387
45. Assumpcao L, Choti M, Pawlik TM, Gecshwind JF, Kamel IR (2009) Functional MR imaging as a new paradigm for image guidance. Abdom Imaging 34:675–685
46. Schraml C, Schwenzer NF, Clasen S, et al. (2009) Navigator respiratory-triggered diffusion-weighted imaging in the follow-up after hepatic radiofrequency ablation-initial results. J Magn Reson Imaging 29:1308–1316
47. Pupulim LF, Hakime A, Barrau V, et al. (2009) Fatty hepatocellular carcinoma: radiofrequency ablation–imaging findings. Radiology 250:940–948
48. Cho YK, Kim JK, Kim MY, Rhim H, Han JK (2009) Systematic review of randomized trials for hepatocellular carcinoma treated with percutaneous ablation therapies. Hepatology 49:453–459
49. Sironi S, De Cobelli F, Livraghi T, et al. (1994) Small hepatocellular carcinoma treated with percutaneous ethanol injection: unenhanced and gadolinium-enhanced MR imaging follow-up. Radiology 192:407–412
50. Ebara M, Kita K, Sugiura N, et al. (1995) Therapeutic effect of percutaneous ethanol injection on small hepatocellular carcinoma: evaluation with CT. Radiology 195:371–377
51. Rimassa L, Santoro A (2009) Sorafenib therapy in advanced hepatocellular carcinoma: the SHARP trial. Expert Rev Anticancer Ther 9:739–745
52. Horger M, Lauer UM, Schraml C, et al. (2009) Early MRI response monitoring of patients with advanced hepatocellular carcinoma under treatment with the multikinase inhibitor sorafenib. BMC Cancer 9:208
53. Maksimovic O, Schraml C, Hartmann JT, et al. (2010) Evaluation of response in malignant tumors treated with the multitargeted tyrosine kinase inhibitor sorafenib: a multitechnique imaging assessment. AJR Am J Roentgenol 194:5–14